Chemistry & Biology 13, 765–770, July 2006  DOI 10.1016/j.chembiol.2006.05.012

# Discovery of Bioactive Small-Molecule Inhibitor of Poly ADP-Ribose Polymerase: Implications for Energy-Deficient Cells

**Stephen M. Altmann,[1] Andrey Muryshev,[2,3] Elisa Fossale,[4] Michele M. Maxwell,[1] Francine N. Norflus,[1] Jonathan Fox,[1] Steven M. Hersch,[1] Anne B. Young,[1] Marcy E. MacDonald,[4] Ruben Abagyan,[5] and Aleksey G. Kazantsev[1,*]**

[1] Massachusetts General Institute for Neurodegenerative Disease and Harvard Medical School
Department of Neurology
Massachusetts General Hospital
Harvard Medical School
Building 114, 3300 16th Street
Charlestown, Massachusetts 02129

[2] 123182, Institute of Molecular Physics
Kurchatov Square 1
Moscow
Russia

[3] Molsoft LLC
3366 North Torrey Pines Court
Suite 300
La Jolla, California 92037

[4] Richard B. Simches Research Center
185 Cambridge St.
Boston, Massachusetts 02114

[5] Department of Molecular Biology
The Scripps Research Institute
10550 North Torrey Pines Road
La Jolla, California 92037

## Summary

**Poly (ADP-ribose) polymerase (PARP1) is a nuclear protein that, when overactivated by oxidative stress-induced DNA damage, ADP ribosylates target proteins leading to dramatic cellular ATP depletion. We have discovered a biologically active small-molecule inhibitor of PARP1. The discovered compound inhibited PARP1 enzymatic activity in vitro and prevented ATP loss and cell death in a surrogate model of oxidative stress in vivo. We also investigated a new use for PARP1 inhibitors in energy-deficient cells by using Huntington's disease as a model. Our results showed that insult with the oxidant hydrogen peroxide depleted cellular ATP in mutant cells below the threshold of viability. The protective role of PARP1 inhibitors against oxidative stress has been shown in this model system.**

## Introduction

The products of oxidative stress, various oxidants, and free radicals induce DNA strand breaks, triggering PARP1 activation [1]. PARP1, one of the most abundant proteins in the nucleus, can be activated up to 100-fold by damaged DNA [2, 3]. This enzyme, which catalyzes the synthesis of poly ADP-ribose polymers on acceptor proteins with $NAD^+$ as substrate, is primarily responsible for the catastrophic $NAD^+$ and ATP loss observed under conditions of high oxidative stress [4, 5]. In the absence of functional PARP1, DNA base excision repair is delayed after exposure of cells to ionizing radiation or alkylating agents [6]. Over activated PARP1 may even cause necrosis by depleting cellular energy sources beneath the threshold of survival [7]. The use of bioenergetic molecules ($NAD^+$) to build up biopolymers (poly-ADP-ribose) in a highly processive manner for the purpose of structural interference and signal transduction suggests a unique role for PARP1 in cellular energy balance and viability. A therapeutic approach, based on the pharmacological inhibition of PARP1, was proposed for a diverse and large group of human disorders. Here, we report the discovery of a novel bioactive small-molecule inhibitor of PARP1 and the therapeutic application of PARP1 inhibitors for metabolically impaired cells.

## Results and Discussion

### Identification of a Novel PARP1 Inhibitor

We performed an in silico search of biologically active scaffolds from our in-house compound library that have been previously identified and examined in various cell-based assays. Through this approach, we hoped to limit our search to only those scaffolds that are known to be active in a cell-based system, thus eliminating scaffolds that are toxic or not cell penetrable. In conducting this search, we identified two candidate compounds, CG1 and K245-14, with structural properties shared by known PARP1 inhibitors (Figure 1A). Docking these two compounds to the PARP1 active site with the ICM program [8], we have obtained docking score values lying in the same range as those of a selection of known PARP1 inhibitors that we used as a reference (Figure 1H). Moreover, the positions that the CG1 and K245-14 occupy in the binding pocket are highly similar to the positions of cocrystallized PARP1 ligands presented in PDB. In particular, the amino group in these two molecules makes hydrogen bonds to Ser-243 and Gly-202 (Figure 1I), which was suggested to be key for PARP-1 inhibition [9], and aromatic rings are enclosed between rings of Glu-179 and Tyr-235 (residue numbering form PDB entry 1uk0 is used throughout this paper).

To determine if CG1 and K245-14 had PARP1 inhibitory activity, we tested them in an in vitro PARP1 enzyme assay, and they demonstrated inhibitory effects in a dose-dependent manner (Figure 1B). CG1 and K245-14 yielded $IC_{50}$ values of 2.5 μM and 2.0 μM, respectively (Figures 1C and 1H).

We then attempted to find more potent PARP1 inhibitors, focusing ourselves on optimization of K245-14. The 3D structure of K245-14 docked to the binding pocket hinted to two directions of the lead optimization. The first, more straightforward one is to modify aliphatic side group of the molecule. It is this direction that we pursued in the present study. From a database of available molecules, we selected seven analogs of K245-14

*Correspondence: akazantsev@partners.org

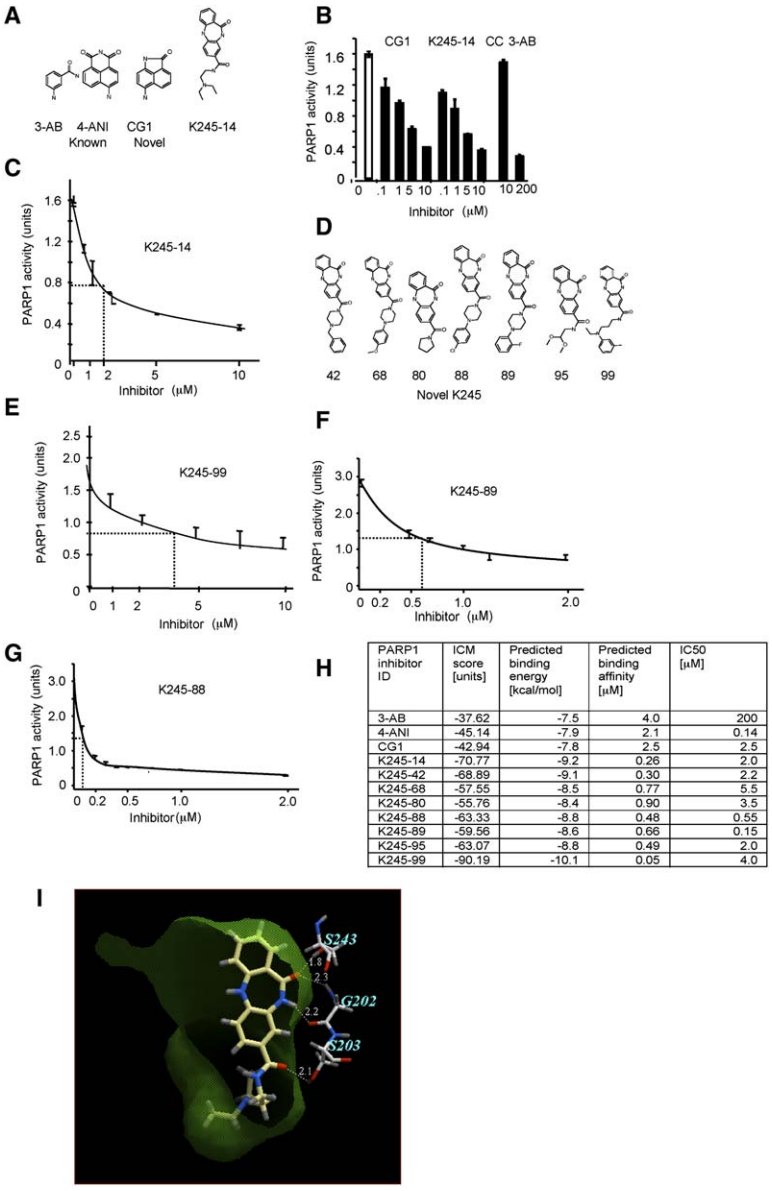


| PARP1 inhibitor ID | ICM score [units] | Predicted binding energy [kcal/mol] | Predicted binding affinity [μM] | IC50 [μM] |
|---|---|---|---|---|
| 3-AB | -37.62 | -7.5 | 4.0 | 200 |
| 4-ANI | -45.14 | -7.9 | 2.1 | 0.14 |
| CG1 | -42.94 | -7.8 | 2.5 | 2.5 |
| K245-14 | -70.77 | -9.2 | 0.26 | 2.0 |
| K245-42 | -68.89 | -9.1 | 0.30 | 2.2 |
| K245-68 | -57.55 | -8.5 | 0.77 | 5.5 |
| K245-80 | -55.76 | -8.4 | 0.90 | 3.5 |
| K245-88 | -63.33 | -8.8 | 0.48 | 0.55 |
| K245-89 | -59.56 | -8.6 | 0.66 | 0.15 |
| K245-95 | -63.07 | -8.8 | 0.49 | 2.0 |
| K245-99 | -90.19 | -10.1 | 0.05 | 4.0 |

Figure 1. Identification of Novel PARP1 Inhibitor Scaffolds

(A) Structures of known PARP1 inhibitors used to screen in-house library and the two novel structures found in the screen.

(B) In vitro PARP1 enzyme assay with two novel structures and 3AB as a control.

(C) $IC_{50}$ curve of K245-14.

(D) Analogs of K245-14 that showed PARP1 inhibition.

(E–G) $IC_{50}$ curves of selected structures from K245 series.

(H) Predicted versus measured values of binding affinity for PARP-1 inhibitors. The third and fourth columns are computed on the basis of docking score values (second column, see Experimental Procedures section for details), and the fifth column contains experimentally measured IC50 values.

(I) K245-14 docked to human PARP-1 active site. The binding pocket is schematically represented by its solvent accessible surface. Dashed lines indicate hydrogen bonds. Error bars represent the standard deviation of the mean of three replicates.

with variations in the desired group. Docking studies of these molecules provided positions and docking score values close to those of K245-14, indicating that the molecules are likely to bind to PARP1. In enzyme-inhibition assays, all the molecules demonstrated PARP1 inhibition, with the best inhibitor providing 10-fold increase in potency over the original K245-14 compound (Figures 1E–1H).

### Demonstration of Activity in Cultured Cells

Having demonstrated the in vitro inhibition of PARP1 by CG1 and the K245 series, we sought to assess the biological activity of these new entities in a relevant cell-based assay. The ability of PARP1 inhibitors to prevent cellular ATP depletion under conditions of oxidative stress is well documented [4, 10, 11]. In a surrogate model of oxidative stress, cellular PARP1 is activated in response to exposure of cells to hydrogen peroxide. First, we validated the oxidative stress model of PARP1 activation with the known inhibitor 4-ANI. This highly potent PARP1 inhibitor ($IC_{50}$ = 180 nM) rescued oxidant-dependent ATP loss in human (HeLa) and rat pheochromocytoma (PC12) cell lines (Figures 2A and 2B). Next, we assessed cell viability by measuring the activity of mitochondrial dehydrogenases in a modified MTT assay that utilizes the reagent WST-1. Mitochondrial dehydrogenases are not regulated by the PARP1 pathway, thus providing an objective cell viability read out independent from PARP1 activation or inhibition. We demonstrated hydrogen peroxide-dependent loss of cell viability in both HeLa and PC12 cell lines and rescue of viability loss with 4-ANI (Figures 2C and 2D). As anticipated, we observed a good correlation between loss of ATP and viability in both cell lines, with 4-ANI showing efficacy in both ATP and WST-1 assays in HeLa and in PC12 cells.

After establishing the cellular oxidative stress model, we tested CG-1 and the K245 series of active inhibitors. Surprisingly, only compound K245-14 demonstrated consistent and notable rescue in both assays (Figures

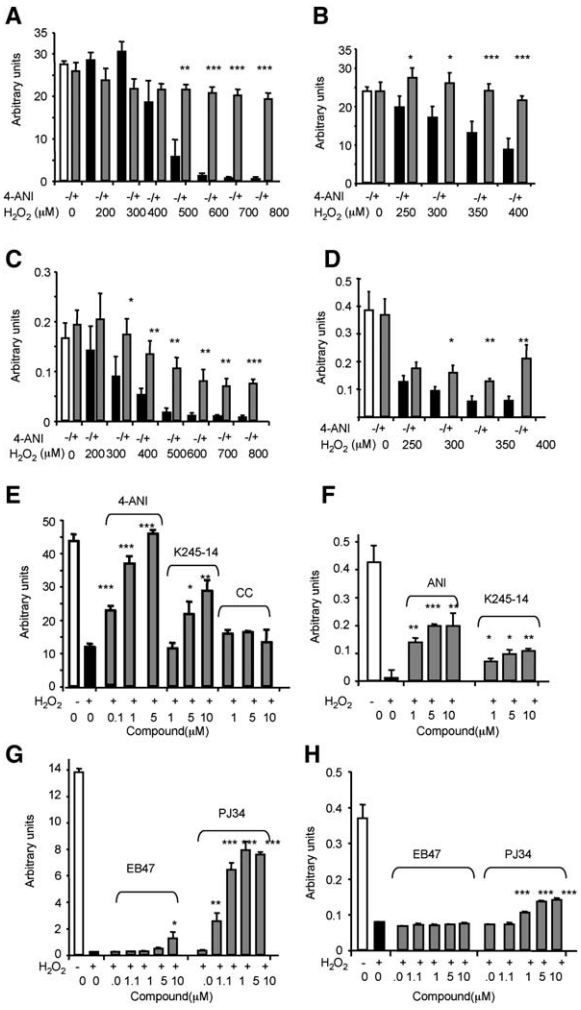


Figure 2. Novel PARP1 Inhibitor Rescues Peroxide-Induced Loss of ATP and Cell Viability

(A) HeLa cells treated with various concentrations of $H_2O_2$ for 2 hr (±) pretreatment for 1 hr with 4-ANI after which cells were assayed for total ATP levels.

(B) Same as in (A) except with PC12 cells.

(C) HeLa cells were treated with various concentrations of $H_2O_2$ for 2 hr (±) pretreatment for 1 hr with 4-ANI after which 1/10 cell culture volume of WST1 reagent was added. Cells were incubated for 1 hr after which Abs450 was measured.

(D) Same as in (C) except with PC12 cells.

(E) ATP assay on PC12 cells pretreated for 1 hr with the indicated compounds, followed by exposure to 400 μM $H_2O_2$ for 2 hr.

(F) WST1 assay on PC12 cells pretreated for 1 hr with the indicated compounds, followed by exposure to 400 μM $H_2O_2$ for 2 hr.

(G) ATP assay on PC12 cells with potent in vitro PARP1 inhibitors.

(H) WST1 assay on PC12 cells treated with the same inhibitors. Asterisk, $p < 0.05$; double asterisk, $p < 0.01$; triple asterisk, $p < 0.001$ versus peroxide only treatment.

Error bars represent the standard deviation of the mean of three replicates.

2E and 2F). Rescue of ATP by K245-88, the most potent analog of K245-14, showed slight rescue only under conditions of severe oxidation (data not shown). We extended our tests to two known highly potent in vitro PARP1 inhibitors EB47 ($IC_{50}$ = 45 nM) and PJ34 ($IC_{50}$ = 20 nM). While EB47 failed to block ATP depletion and rescue viability loss, PJ34 was highly effective in both assays (Figures 2G–2H). The effects of K245-14 and PJ34 were similar in magnitude, with both compounds rescuing 50% of ATP depletion and 25% of viability loss. Viability tests on K245-14 from 0.01–25 μM did not reveal any apparent loss of viability. We have advanced K245-14 as a lead compound for further potency and ADMET optimization. Our results suggest, however, that high potency of PARP1 inhibition in vitro does not necessarily lead to a robust biological response. Using the tools of computational chemistry, we envision the rational optimization of lead compound K245-14, followed by empirical testing in in vitro and cell-based assays.

Our data provide the basis for development of a screening platform to search for bioactive small-molecule PARP1 inhibitors, utilizing the oxidant treatment of cells combined with ATP rescue or cell viability readouts. This approach has been validated in a pilot screen of 2000 compounds to demonstrate the feasibility of a cell-based screen for PARP1 inhibitors (data not shown).

## Application of PARP1 Inhibitors for Energy-Deficient Cells

Next, we set out to explore new therapeutic applications for PARP1 inhibitors. We reasoned that metabolically impaired and energy-deficient cells will be more vulnerable to robust ATP depletion, mediated by activated PARP1, than normal counterparts. In cells where ATP levels are already lower than normal due to, for example, mitochondrial impairment, activation of PARP1 may seriously compromise cellular functions and viability [12].

In Huntington's disease (HD), an autosomal dominant disorder, mitochondrial dysfunction and ATP deficiency have been implicated in disease pathology; however, the precise mechanism(s) of neurodegeneration remains elusive [13]. Huntington's disease is characterized by progressive neuronal cell loss in the striatum and the cortex. Energy deficits likely compound the influence of molecular and environmental stresses and increase the vulnerability of neurons in HD [14]. PARP1 activation, in response to DNA damage caused by oxidative stress or by intracellular oxidation, may lead to further decrease of ATP levels below the threshold of normal cell function and viability in energy-deficient mutant HD cells [15, 16, 17]. Appropriate PARP1 activation as a component of cellular defense mechanisms in wild-type cells makes energy-deficient HD cells vulnerable due to unsustainable loss of ATP. Hence, we propose that prevention of ATP loss in energy-deficient mutant HD cells with small-molecule inhibitors of PARP1 may provide therapeutic benefits and should be tested.

To this end, we have assessed the ability of 4-ANI and K245-14 to prevent ATP loss in human Huntington's disease and normal lymphoblastoid cells, as well as in mutant and wild-type mouse striatal cells (Figures 3A–3D). We also observed the previously reported reduced ATP levels in all mutant cell lines relative to normal controls [18]. Treatment of cells with the oxidant $H_2O_2$ caused ATP loss in both wild-type and mutant cells. While the small-molecule inhibitors 4-ANI and K245-14 prevented the loss of ATP in both mutant and normal murine and human cells, the benefits of PARP1 inhibition for severely energy-depleted HD cells were readily apparent (Figures 3A, 3B, and 3D). Absolute rescued residual ATP levels in treated cells were dependent on

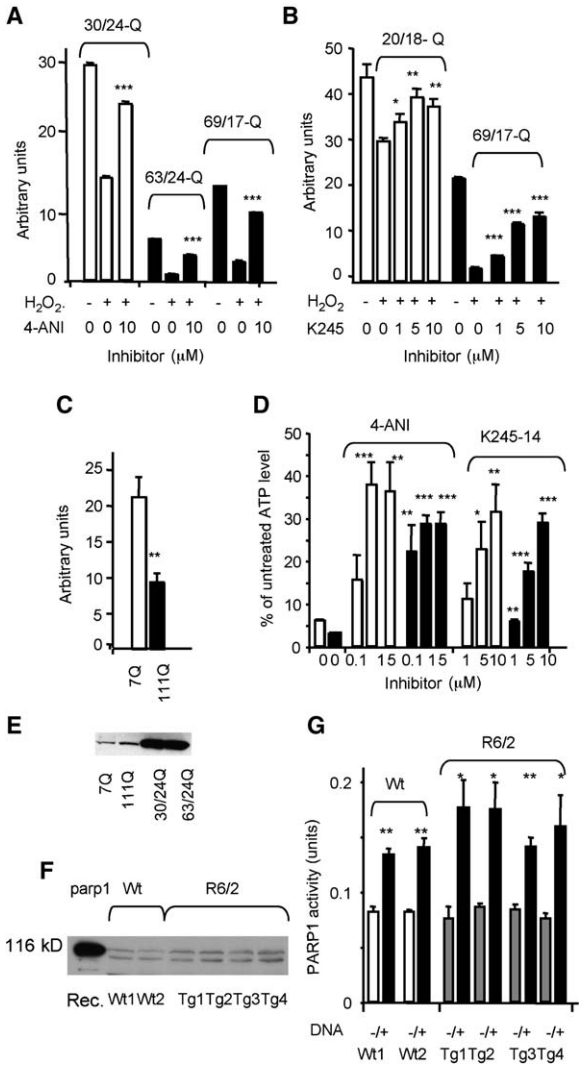


Figure 3. Use of HD as a Model for Potentially Novel Application for PARP1 Inhibitors

(A) Effect of 10 μM 4-ANI preincubated for 1 hr on ATP levels in wild-type (white bars) and two mutant HD (black bars) lymphoblastoid cell lines with (+) or without (−) 200 μM $H_2O_2$ for 2 hr. Triple asterisk, $p < 0.001$ versus $H_2O_2$ alone treated cells.

(B) Wild-type (white bars) and mutant (black bars) lymphoblastoid cells preincubated with K245-14 for 1 hr, followed by treatment with (+) or without (−) 200 μM $H_2O_2$ for 2 hr. Asterisk, $p < 0.05$; double asterisk, $p < 0.01$; triple asterisk, $p < 0.001$ versus $H_2O_2$ alone treated cells.

(C) Basal ATP levels in wild-type ST*Hdh*$^{Q7/Q7}$ and mutant ST*Hdh*$^{Q111/Q111}$ striatal cells.

(D) Wild-type (white bars) and mutant (black bars) striatal cells preincubated with indicated compounds for 1 hr followed by treatment with 400 μM $H_2O_2$ for 2 hr. Asterisk, $p < 0.05$; double asterisk, $p < 0.01$; triple asterisk, $p < 0.001$ versus $H_2O_2$ alone treated cells.

(E) PARP1 protein levels in untreated wild-type ST*Hdh*$^{Q7/Q7}$ and mutant ST*Hdh*$^{Q111/Q111}$ striatal cells, and in wild-type (30/24 CAG), and mutant HD (63/24 CAG) lymphoblastoid cells.

(F) Western blot of PARP1 expression in wild-type and R6/2 transgenic mouse cortexes alongside recombinant PARP1 (lane 1).

(G) PARP1 enzyme activity levels for wild-type and transgenic mouse cortexes. For this assay, mouse cortex extracts were used in place of recombinant PARP1 in the standard enzyme assay. Asterisk, $p < 0.05$; double asterisk, $p < 0.01$ versus no DNA activation.

Error bars represent the standard deviation of the mean of three replicates.

the basal ATP levels in unstressed mutant and wild-type cells, compound potencies of PARP1 inhibitors (Figures 3A–3D), and the severity of the stress as defined by $H_2O_2$ concentrations (not shown). Similar results were achieved in cells treated with the DNA-damaging agent methyl nitrosourea (MNU), although ATP loss in HD and wild-type cells was not robust and significant only at high concentration (5 mM) of MNU. Notably, the inhibitors were ineffective in preventing ATP loss mediated by the mitochondrial toxin, 3-nitropropionic acid (3-NP) when using ST*Hdh*$^{Q7/Q7}$ and ST*Hdh*$^{Q111/Q111}$ striatal cells [19], demonstrating specificity for PARP1 inducing agents (not shown). Since the basis for the mitochondrial defect in Huntington's disease is unknown, we limited our experiments to measurement of PARP1-dependent ATP levels and did not include the mitochondrial dehydrogenase-dependent WST-1 assay. We have measured and detected no effect of PARP1 inhibitors on basal ATP levels in normal and HD lymphoblastoid cells or in wild-type and mutant striatal cells in the absence of induced PARP1 activation. This suggests that PARP1 activity is not responsible for mitochondrial defects and the reduction of basal ATP levels. Furthermore, we have not discovered differences in PARP1 protein levels (Figure 3E), in PARP1 basal activities, and in rate of PARP1 activation in mutant HD and normal cells (not shown). However, in both striatal cell lines PARP1 expression levels were quite low, which might explain their resistance to high concentrations of $H_2O_2$ (data not shown). Further, we have tested PARP1 levels in mouse cortexes, the brain area affected in Huntington's disease. Extracts were prepared from cortexes of wild-type and HD transgenic R6/2 mice, sacrificed at 80 days, when the process of neurodegeneration has started. We did not observe any difference in the level of PARP1 expression between wild-type and HD samples (Figure 3F). The observed doublet at 116 kDa may be attributable to posttranslational modification. A faint band was observed at 85 kDa (not shown), indicative of PARP1 cleavage, although this band was equally present in both wild-type and transgenic samples. Finally, we tested and observed the same magnitude of PARP1 activation in wild-type and HD cortex extracts, supplemented with damaged DNA (Figure 3G). These data suggest that HD cells have normal functional PARP1, which upon activation can deplete ATP levels of mutant cells further below the threshold of viability.

Small-molecule inhibitors effectively protect HD cells from PARP1-dependent energy depletion, triggered by stimuli such as oxidative stress. Our results suggest that PARP1 activation could be a significant contributing factor to the pathological reduction of energy resources that occurs in HD. To assess the therapeutic potential of PARP1 pharmacological inhibition, we propose optimizing lead compound K245-14 for potency and ADMET, conduct pharmacology studies, and advance selected analogs to efficacy trials in HD mouse models.

## Significance

**PARP1 was proposed as a useful drug target for a broad and diverse group of human disorders. To identify bioactive small-molecule inhibitors of PARP1, we**

**performed an in silico search of biologically active scaffolds that we have previously identified and examined in various cell-based assays. By conducting a search, we identified candidate compounds belonging to two novel scaffolds that demonstrated PARP1 inhibition activity in vitro. To demonstrate the biological activity of our novel inhibitors, we developed two PARP1-dependent cell-based assays. The experiments yielded a lead compound, performing in live cells consistently and selectively with respect to inhibition of PARP1 target. Notably, not all highly potent in vitro known PARP1 inhibitors also tested were biological active. Furthermore, magnitudes of biological effects were the same for known and novel PARP1 inhibitors, suggesting that biological activities in vivo depend on other important properties of small molecules and are not limited to high potency of inhibition in vitro. Based on our results, we proposed to identify novel bioactive small molecules by using a cell-based screening platform, which utilizes oxidant treatment of cells combined with ATP rescue or cell viability read outs. Further, we explored a new therapeutic application for PARP1 inhibitors in metabolically impaired and energy-deficient cells. Huntington's disease cells from patients and transgenic mice showed energy deficiency due to mitochondrial impairment. Low basal ATP levels in mutant cells made them more sensitive than normal counterparts to robust energy depletion, mediated by PARP1. We demonstrated significant reduction of ATP levels in mutant cells in response to oxidant treatment and rescue of energy depletion with PARP1 inhibitors. Novel and known inhibitors selectively protected cells against acute oxidative stress. Lastly, we have shown that PARP1 was functional in brain extracts from transgenic HD, and therefore, pharmacological inhibition of PARP1 activation could be neuroprotective.**

## Experimental Procedures

### Compounds

Chemical entities CG1 (MW 184, H_acceptors 1, H_donors 3, logP 0.94, logD 1.34, logSw −1.74) and K245-14 (MW 352, H_acceptor 3, H_donors 3, logP2.37, logD 1.05, logSw −0.083) for study were synthesized at and obtained from Chemical Diversity (San Diego). PARP1 inhibitors 3-AB and 4-ANI were purchased from Trevigen and Calbiochem respectively.

### Cell Culture

HeLa cells were cultured in DMEM with 10% FBS. Human lymphoblast cells derived from HD patients carrying either one mutant and one wild-type HD allele (69/17 CAG and 63/24 CAG) or two wild-type alleles (20/18 CAG and 30/24 CAG) were cultured in RPMI 1640 with 10% FBS, 2 mM L-glutamine, and 100 μg/ml penicillin/streptomycin. STHdh$^{Q7/Q7}$ and ST*Hdh*$^{Q111/Q111}$ striatal cells, expressing endogenous mutant huntingtin with 111-glutamines or endogenous wild-type huntingtin with 7-glutamines, respectively, have been described elsewhere [20]. Previously reported PC12 cells with an integrated HD103Q-EGFP construct, expressing the first 17 N terminus amino acids of huntingtin with 103 glutamines, tagged with EGFP, were cultured in DMEM containing 10% horse serum, 5% FBS, 2 mM L-glutamine, 200 μg/ml G418, and 100 μg/ml zeocin. Lymphoblast and PC12 cultures were kept at 37°C and 5% $CO_2$ in a humidified chamber.

### High-Throughput Screening

High-throughput screen was carried out with a 1860 compound library from Timtec consisting of naturally derived products. Compounds were dispensed into assay plates with an EP3 liquid handler (PerkinElmer), and plates were read on a Wallac Victor$^2$V plate reader (PerkinElmer).

### ATP Assay

For determinations of ATP levels in PC12, lymphoblastoid, and striatal cells, cells were plated to 50% confluency in 96-well plates and allowed to attach, after which cells were treated with various concentrations of either hydrogen peroxide ($H_2O_2$) diluted in PBS, 3-nitropropionic acid (3-NP) dissolved in PBS/0.2N NaOH to 200 mM to keep the pH neutral, or methyl nitrosourea (MNU) dissolved in PBS to 100 mM. ATP measurements were performed with cells treated with hydrogen peroxide for 2 hr, with 3-NP for 2, 24, 48, and 72 hr, and with MNU for 1, 2, and 6 hr. Lymphoblastoid cells were plated in 24-well plates and incubated with the stress inducing agents for 2 hr. Cells were pelleted prior to lysis. After incubation with stress inducing reagents, the cells were lysed in RIPA buffer, and total protein quantified with the BCA protein assay kit (Pierce). Triplicate aliquots of normalized extract were mixed with equal volumes of ATPlite reagent, and luminescence measured in a Victor$^2$V plate reader.

The CellTiter GLO Luminescent cell viability kit (Promega) was used for the determination of ATP levels in the NP3-treated striatal cells. 20,000 cells/well were plated in a black opaque-walled 96-well plate (Packard Bioscience) and incubated overnight. The cells were then treated with different concentrations of K245-14 and 4-ANI, in presence or absence of 1 mM 3-NP for 48 hr, adjusting the concentration of mock (DMSO) to 0.1% for all the treatments. Following the incubation, cell lysis was induced by adding CellTiter-GLO reagent to each well and mixing on a shaker for 2 min. An ATP standard curve was prepared in the same plate. The plate was dark adapted for 10 min to stabilize the luminescence signal, which was then recorded with a microplate luminometer (MicroLumat Plus LB 96V, Berthold Technologies) with a 30 s recording time.

### PARP Assay

PARP assays were carried out with the Universal Colorimetric PARP activity assay kit (Trevigen) according to the manufacturer's instructions. To measure the basal PARP1 activities in the enzymatic assay, the cell extracts were not supplemented with exogenous damaged DNA.

### Western Blot Analysis

To determine cellular levels of PARP protein, cells were lysed for 30 min on ice in PARP buffer containing 0.3 M NaCl, 1 mM PMSF, and a protease inhibitor cocktail. Lysates were then centrifuged for 10 min at 10,000 × g, and the resulting supernatant quantified by BCA. Twenty-five milligrams of protein was loaded and separated on a 10% polyacrylamide gel. Samples were transferred to a PVDF membrane, blocked in 5% nonfat milk in PBST, and probed with an anti PARP MAb (C2-10, Trevigen) at 1:2000. Blots were washed with PBST and probed with an HRP-conjugated anti-mouse secondary antibody and visualized by using ECL.

### Molecular Modeling

In the Protein Data Bank (PDB), there are three X-ray structures of human PARP1 having resolution 3Å (PDB codes: 1UK0, 1UK1, and 1WOK) and seven X-ray structures of nonhuman PARP1 from which the structure 1A26 representing chicken PARP1 has the best resolution of 2.25Å. To take favor of both structure identity and higher resolution, in this study, we used both human (1UK0) and chicken (1A26) 3D structures for molecular docking. For the molecular modeling calculations, we used ICM program (reference is given above). The binding site was identified with ICM binding pocket location algorithm. In the 1A26 structure, the only side chain in the binding site that differs from that of human PARP1 is GLN-673. We mutated it numerically to glutamic acid to mimic human PARP1. For both 3D structures, we minimized side chained with ICM biased probability Monte Carlo method [21] and then minimized the entire structures with ICM local minimization in the presence of native ligand contained in 1UK0. We performed docking of the studied molecules to both of the structures. The docking score values obtained with the two structures are very close to each other with linear correlation coefficient $R^2$ = 0.96. In this paper, we present only docking score

values obtained with 1UK0 structure. To determine a characteristic scale of docking score for PARP1 inhibitors, we docked ten known inhibitors to the PARP1 binding site (structures not presented). These reference inhibitors exhibited score values in the range from 35 to 100 ICM score units. We used the obtained score values to calibrate ICM docking score to the experimental binding energy values by linear transformation $E = A\,S + B$, where $S$ is ICM score and A and B are constants determined by least squares fit of the score values to binding energies. We used the following approximate relation between binding energy and binding affinity: $E = \mathrm{Log}_{10}(K_d/1\ \mathrm{Mol}) \times 1.4$ kcal/Mol, binding affinity being given by dissociation constant $K_d$.

### Statistics

Experiments were repeated two to three times, and a representative example is shown. Significance values between samples were obtained by the Student's t test with p values < 0.05 (marked with an asterisk) considered significant (double asterisk, p < 0.01; triple asterisk, p < 0.001); for all p values, n = 3. Values are represented as the mean ± SD.

### Acknowledgments

Supported by National Institutes of Health grants NS32765, NS16367, and GM071872-02, and the Huntington's Disease Society of America Coalition for the Cure Energy Team (M.E.M.).

Received: October 5, 2005
Revised: May 22, 2006
Accepted: May 23, 2006
Published: July 28, 2006

### References

1. Berger, N.A., Whitacre, C.M., Hashimoto, H., Berger, S.J., and Chatterjee, S. (1995). NAD and poly(ADP-ribose) regulation of proteins involved in response to cellular stress and DNA damage. Biochimie *77*, 364–367.
2. Chatterjee, S., Berger, S.J., and Berger, N.A. (1999). Poly(ADP-ribose) polymerase: a guardian of the genome that facilitates DNA repair by protecting against DNA recombination. Mol. Cell. Biochem. *193*, 23–30.
3. D'Amours, D., Desnoyers, S., D'Silva, I., and Poirier, G.G. (1999). Poly(ADP-ribosyl)ation reactions in the regulation of nuclear functions. Biochem. J. *342*, 249–268.
4. Jagtap, P., and Szabo, C. (2005). Poly(ADP-ribose) polymerase and the therapeutic effects of its inhibitors. Nat. Rev. Drug Discov. *4*, 421–440.
5. Cole, K.K., and Perez-Polo, J.R. (2002). Poly(ADP-ribose) polymerase inhibition prevents both apoptotic-like delayed neuronal death and necrosis after H(2)O(2) injury. J. Neurochem. *82*, 19–29.
6. Dantzer, F., de La Rubia, G., Menissier-De Murcia, J., Hostomsky, Z., de Murcia, G., and Schreiber, V. (2000). Base excision repair is impaired in mammalian cells lacking Poly(ADP-ribose) polymerase-1. Biochemistry *39*, 7559–7569.
7. Ying, W., Alano, C.C., Garnier, P., and Swanson, R.A. (2005). NAD+ as a metabolic link between DNA damage and cell death. J. Neurosci. Res. *79*, 216–223.
8. Abagyan, R., Totroy, M., and Kuznetsov, D. (2004). ICM—a new method for protein modeling and design: applications to docking and structure prediction from the distorted native conformation. J. Comp. Chem. *15*, 488–506.
9. Cepeda, V., Fuertes, M.A., Castilla, J., Alonso, C., Quevedo, C., Soto, M., and Pérez, J.M. (2006). Poly(ADP-ribose) polymerase-1 (PARP-1) inhibitors in cancer chemotherapy. Recent Pat. Anticancer Drug Discov. *1*, 39–53.
10. Iwashita, A., Tojo, N., Matsuura, S., Yamazaki, S., Kamijo, K., Ishida, J., Yamamoto, H., Hattori, K., Matsuoka, N., and Mutoh, S. (2004). A novel and potent poly(ADP-ribose) polymerase-1 inhibitor, FR247304 (5-chloro-2-[3-(4-phenyl-3,6-dihydro-1(2H)-pyridinyl)propyl]-4(3H)-quinazo linone), attenuates neuronal damage in in vitro and in vivo models of cerebral ischemia. J. Pharmacol. Exp. Ther. *310*, 425–436.
11. Calabrese, C.R., Almassy, R., Barton, S., Batey, M.A., Calvert, A.H., Canan-Koch, S., Durkacz, B.W., Hostomsky, Z., Kumpf, R.A., Kyle, S., et al. (2004). Anticancer chemosensitization and radiosensitization by the novel poly(ADP-ribose) polymerase-1 inhibitor AG14361. J. Natl. Cancer Inst. *96*, 56–67.
12. Grunewald, T., and Beal, M.F. (1999). Bioenergetics in Huntington's disease. Ann. N Y Acad. Sci. *893*, 203–213.
13. Ross, C.A. (2002). Polyglutamine pathogenesis: emergence of unifying mechanisms for Huntington's disease and related disorders. Neuron *35*, 819–822.
14. Polidori, M.C., Mecocci, P., Browne, S.E., Senin, U., and Beal, M.F. (1999). Oxidative damage to mitochondrial DNA in Huntington's disease parietal cortex. Neurosci. Lett. *272*, 53–56.
15. Browne, S.E., Ferrante, R.J., and Beal, M.F. (1999). Oxidative stress in Huntington's disease. Brain Pathol. *9*, 147–163.
16. Browne, S.E., Bowling, A.C., MacGarvey, U., Baik, M.J., Berger, S.C., Muqit, M.M., Bird, E.D., and Beal, M.F. (1997). Oxidative damage and metabolic dysfunction in Huntington's disease: selective vulnerability of the basal ganglia. Ann. Neurol. *41*, 646–653.
17. Giuliano, P., De Cristofaro, T., Affaitati, A., Pizzulo, G.M., Feliciello, A., Criscuolo, C., De Michele, G., Filla, A., Avvedimento, E.V., and Varrone, S. (2003). DNA damage induced by polyglutamine-expanded proteins. Hum. Mol. Genet. *12*, 2301–2309.
18. Seong, I.S., Ivanova, E., Lee, J.-M., Choo, Y.S., Fossale, E., Anderson, M., Gusella, J.F., Laramie, J.M., Myers, R.H., Lesort, M., and MacDonald, M.E. (2005). HD CAG repeat implicates a dominant property of huntingtin in mitochondrial energy metabolism. Hum. Mol. Genet. *14*, 2871–2880.
19. Gines, S., Seong, I.S., Fossale, E., Ivanova, E., Trettel, F., Gusella, J.F., Wheeler, V.C., Persichetti, F., and MacDonald, M.E. (2003). Specific progressive cAMP reduction implicates energy deficit in presymptomatic Huntington's disease knock-in mice. Hum. Mol. Genet. *12*, 497–508.
20. Trettel, F., Rigamonti, D., Hilditch-Maguire, P., Wheeler, V.C., Sharp, A.H., Persichetti, F., Cattaneo, E., and MacDonald, M.E. (2000). Dominant phenotypes produced by the HD mutation in STHdh(Q111) striatal cells. Hum. Mol. Genet. *9*, 2799–2809.
21. Abagyan, R., and Totrov, M. (1994). Biased probability Monte Carlo conformational searches and electrostatic calculations for peptides and proteins. J. Mol. Biol. *235*, 983–1002.